A&A 407, 503–513 (2003)
DOI: 10.1051/0004-6361:20030751

Astronomy & Astrophysics

Chandra observations of the X-ray environment of BL Lacs

D. Donato[1], M. Gliozzi[2], R. M. Sambruna[1,2], and J. E. Pesce[2,3]

[1] George Mason University, School of Computational Sciences, 4400 University Drive, Fairfax, VA 22030, USA
[2] George Mason University, Dept. of Physics & Astronomy, MS 3F3, 4400 University Drive, Fairfax, VA 22030, USA
[3] Eureka Scientific

Received 17 February 2003 / Accepted 13 May 2003

Abstract. We present *Chandra* observations of the X-ray environment of a sample of 6 BL Lacertae objects. The improved sensitivity of the ACIS experiment allows us to separate the core X-ray emission from the contribution of diffuse emission from the host galaxy/cluster scales. Within the short (2–6 ks) ACIS exposures, we find evidence for diffuse X-ray emission in 3 sources (BL Lac, PKS 0548–322, and PKS 2005–489). The diffuse emission can be modeled with a King profile with $\beta \sim 0.3{-}0.6$, core radii $r_c \sim 15{-}28$ kpc, and 0.4–5 keV luminosities in the range $10^{41}{-}10^{42}$ erg s^{-1}. In the remaining 3 sources, one (3C 371) has a radial profile entirely consistent with an unresolved source, while two (1ES 2344+514 and 1ES 2321+419) show evidence for weak diffuse emission on kpc scales. These results support current models for radio-loud AGN unifying BL Lacs and FRI radio galaxies through the orientation of their jets. In PKS 0548–322 and PKS 2005–489, we also find evidence for diffuse emission on cluster scales, although the spatial properties of this emission are not constrained. The temperature ($kT \sim 3{-}5$ keV) and luminosity ($L_{0.4-5\ \mathrm{keV}} \sim 10^{42}$ erg s^{-1}) of the cluster gas are typical of normal clusters. Interestingly, these are the two brightest sources of the sample, suggesting a link between environment and nuclear activity.

Key words. galaxies: active – galaxies: fundamental parameters – galaxies: nuclei – X-rays: galaxies

1. Introduction

Orientation-based unification models for Active Galactic Nuclei have been successful in explaining the rich variety of observed properties in the various classes of AGN (Urry & Padovani 1995; Antonucci 1993). According to these schemes, the various AGNs are the same intrinsic object, powered by accretion of the host galaxy gas onto a super-massive black hole, seen at different orientation angles with respect to a preferred axis. In the case of radio-loud AGN, the different subclasses are due to the different orientation of the relativistic jet, with blazars (BL Lacertae objects and Flat Spectrum Radio Quasars) corresponding to the more aligned sources, and radio galaxies (Fanaroff-Riley I and II) being their parent populations (e.g., Urry & Padovani 1995 and references therein).

Previous studies at radio, IR, and optical wavelengths show that for BL Lacs (the relatively local, low-luminosity version of blazars) the parent population is most likely represented by FR I radio galaxies, although some sources may be occasionally hosted by FR IIs (e.g., Kollgaard et al. 1992). Indeed, it is possible to predict the beamed luminosity function of BL Lacs from the luminosity function of FRIs invoking a Lorentz factor $\gamma \sim 3{-}20$, depending on the wavelength (Padovani & Urry 1991; Urry et al. 1991).

Send offprint requests to: D. Donato,
e-mail: davide@physics.gmu.edu

A model-independent probe of these ideas is represented by studies of the near environment. If FRIs are misaligned versions of BL Lacs, the larger-scale environment (host galaxy and cluster of galaxies) of the two classes should be the same, as they are not affected by beaming. Studies at optical-IR wavelengths showed that BL Lacs and FRIs reside in giant elliptical galaxies and, on average, in poor clusters of Abell richness class 0 or less (Falomo et al. 1999; Wurtz et al. 1997).

Similarly, the X-ray environment of BL Lacs and FRIs should be similar. *ROSAT*, and more recently *Chandra*, observations of FRIs established that the X-ray cores of these sources are usually embedded in diffuse soft X-ray emission which is interpreted as the thermal halo of the host galaxy on kpc scales (Worrall et al. 2001; Canosa et al. 1999). However, because of the limited sensitivity and spatial resolution of *ROSAT*, it was not possible to perform similar observations for most BL Lacs, where the bright core dominates the X-ray emission. The only exception is PKS 0521–365, where an unusually large and bright X-ray halo was detected with the *ROSAT* HRI (Hardcastle et al. 1999).

Separating the diffuse X-ray emission from the core X-rays requires high angular resolution and improved sensitivity, such as afforded by the *Chandra* X-ray Observatory (e.g., Birkinshaw et al. 2002). Motivated by these considerations, we acquired *Chandra* imaging observations of a sample of nearby ($z < 0.1$) BL Lacs during cycle 1, to study their kpc-scale X-ray environment and to compare to those of FRIs. As our sample

Table 1. Targets: basic properties.

Object Name (1)	RA (2)	Dec (3)	z (4)	$N_{\rm H,Gal}$ (5)	Type (6)	$L_{2-10\ \rm keV}$ (7)	Ref. (8)
PKS 0548–322	05 50 40.80	–32 16 17.80	0.069	2.52	HBL	31.9	KU98
3C 371	18 06 50.60	+69 49 28.10	0.051	4.73	LBL	1.5	DO01
PKS 2005–489	20 09 25.40	–48 49 54.00	0.071	5.08	HBL	62.2	PA01
BL Lac	22 02 43.30	+42 16 39.80	0.069	21.6	LBL	6.1	RA02
1ES 2321+419	23 23 52.10	+42 10 59.00	0.059	10.9	HBL	1.5	PE96
1ES 2344+514	23 47 04.80	+51 42 17.40	0.044	16.8	HBL	3.9	DO01

Columns: (1) = Source name; (2) = Right Ascension at J2000; (3) = Declination at J2000; (4) = Redshift; (5) = Galactic column density in units of 10^{20} cm^{-2}. The Galactic values was derived from the nh program at HEASARC (based on Dickey & Lockman 1990); (6) = Source type: HBL = High–Energy Peaked BL Lacertae object, LBL = Low–Energy Peaked BL Lacertae object; (7) = Intrinsic X-ray luminosity (in units of 10^{43} erg s^{-1}) between 2 and 10 keV from data in literature; (8) = Reference for the X-ray luminosity: KU98 = Kubo et al. (1998); DO01 = Donato et al. (2001); PA01 = Padovani et al. (2001); RA02 = Ravasio et al. (2002); PE96 = Perlman et al. (1996).

contains sources claimed to reside in optical clusters of galaxies (Falomo et al. 1999), *Chandra* observations can be used to confirm independently the presence of the cluster and quantify physical properties of the intracluster gas.

Based on their spectral energy distributions, BL Lacs can be classified as Low-energy peaked BL Lacs (LBLs), when the radio-to-X-ray spectral index ($\alpha_{\rm rx}$) is larger than 0.75; and as High-energy peaked BL Lacs (HBLs), when $\alpha_{\rm rx} \lesssim 0.75$ (Padovani & Giommi 1995). There is much debate on the origin of the LBL-HBL division, which appears to be continuous with luminosity (Fossati et al. 1997; Sambruna et al. 1996). One of the goals of our GO1 *Chandra* proposal was to investigate whether LBLs and HBLs exist in different X-ray environments, to ascertain whether the ambient gas can affect their different observed jet properties.

The outline of the paper is as follows. In Sect. 2 we discuss the sample selection criteria and in Sect. 3 the observations and data analysis. Results of the spatial and spectral are given in Sects. 4 and 5, respectively. The conclusions are presented in Sect. 6. The analysis of serendipitous X-ray sources is given in Appendix A. Throughout this paper, $H_0 = 75$ km s^{-1} Mpc^{-1} and $q_0 = 0.5$ are adopted. With this choice, $1'$ corresponds to 71 kpc for PKS 0548–322 and for BL Lac, 54 kpc for 3C 371, 73 kpc for PKS 2005–489, 62 kpc for 1ES 2321+419, and 47 kpc for 1ES 2344+514.

2. Sample selection

The targets were selected from two complete, flux-limited samples: the 1 Jy sample of radio-selected L Lacs, and the *Einstein* Slew Survey (1ES) sample of X-ray selected BL Lacs. Sources with redshifts larger than $z = 0.2$ were excluded, to optimize the *Chandra* resolution and for comparison with available samples of FRIs (Worrall et al. 2001). Sources with $z < 0.03$ were also excluded, because the physical size of the field of view is too small to study the intracluster gas ($\leq$0.5 Mpc), should they reside in a cluster of galaxies. In this range we found 4 LBLs in the 1 Jy sample. For each one we chose 2 HBLs matched in redshift (HBLs are more common at low redshifts), in order to have similar redshift distributions for the two types of BL Lacs. The final list contained 12 targets. Only 6 targets were awarded *Chandra* time, including 4 HBLs and 2 LBLs. The targets are listed in Table 1, together with their basic properties and classification.

Imaging data at longer wavelengths are available for all 6 sources, for comparison with the ACIS images. Two of the sources (PKS 0548–322 and PKS 2005–489) are known to reside in a relatively rich optical cluster of galaxies (Falomo et al. 1995; Pesce et al. 1995). The *Chandra* observation of 3C 371, where an X-ray counterpart to the optical jet was found, was previously discussed in Pesce et al. (2001), with main emphasis on the jet properties. Here, we will neglect the X-ray jet for this source and focus on the extended X-ray environment.

3. Observations and data reduction

The *Chandra* observations of the 6 objects were carried out in early 2000. A log of the *Chandra* observations is reported in Table 2, together with information about the source intensities. All sources were observed with ACIS-I at the aimpoint of the I3 chip, except 3C 371 which was observed with ACIS-S, at the aimpoint of S3. The choice of S3 for 3C 371 is due to the fact that it was known to have a synchrotron optical jet. As a science goal for this target was to find the X-ray counterpart of the synchrotron jet, the softer response of a back-illuminated CCD such as S3 was needed to maximize the detection of the X-ray jet.

The short exposures (2–6 ks) were designed to search for the X-ray diffuse emission around the cores, but are clearly insufficient to study in detail their physical properties. Again an exception is 3C 371, where an exposure of 10 ks was requested, in order to detect the X-ray jet (see, e.g., Sambruna et al. 2002).

Since the main purpose of this work is to observe the large-scale environments of blazars, the observations were made with the full CCD operational and the standard ACIS frame time (3.24 s), even if it was expected that the central sources would have produced a high X-ray count rate ($\geq$1 c/s). With this set-up it is likely that more than one photon will be detected in a single CCD pixel within a single integration time. This effect, called pile-up, leads to a distortion (hardening) of the spectrum of the core and a reduction in the measured count

Table 2. Targets: observation log and data.

Object Name (1)	Seq. Num. (2)	Exposure (3)	Start Date (4)	Net Rate (5)	Bkg Rate (6)	c/f (7)
PKS 0548–322	700145	4559	1999/12/31	0.235 ± 0.007	4.71	0.7516
3C 371	700146	10 120	2000/03/21	0.263 ± 0.005	4.56	0.8334
PKS 2005–489	700147	5858	2000/10/07	0.491 ± 0.009	2.61	1.5719
BL Lac	700148	2117	2000/01/07	0.171 ± 0.009	0.14	0.5464
	700196	1039	2000/02/16	0.172 ± 0.013	0.08	–
1ES 2321+419	700149	4628	2000/02/08	0.253 ± 0.007	0.84	0.8114
1ES 2344+514	700150	2727	2000/02/08	0.185 ± 0.008	1.17	0.5912

Columns: (1) = Source name; (2) = Sequence number of the observation; (3) = Net Chandra exposure in seconds after data screening; (4) = Observation start date (Year-Month-Day); (5) = Net photon count rate (c/s) of the source in the energy range 0.3–8 keV; (6) = Background photon count rate (in units of 10^{-3} s^{-1}) obtained rescaling to the same extraction region used for the net source count rate; (7) = Count/frame evaluated with PIMMs and using spectral information from the literature (see previous table for the references). The input flux in PIMMs is such that the output flux corresponds to the measured one.

rate relative to the true incoming rate. Pile-up becomes important for ≥0.1 c/frame.

The pile-up effect also produces an image of the core that is different from the original source image: it appears somewhat extended and flat-topped, and in the cases of most extreme pile-up with a central hole, where the pixels have no counts. In this case the pile-up is strong enough that the total amplitude of the event is larger than the on-board threshold (∼15 keV) and is rejected. This rejection is visible in the images of the central core region of PKS 0548–322 and PKS 2005–489.

For the image analysis we used the `CIAO` 2.2.1 software package and followed the standard reduction criteria, using the latest files provided by the *Chandra* X-ray Center. We inspected the light curves of the background in all cases to search for possible background fluctuations. Only for PKS 0548–322 we found a short variation of the background intensity. The corresponding time interval was removed from the analysis. We restricted our analysis to the 0.3–8.0 keV energy range, where the instrument is better calibrated and the background is negligible.

The exposure for BL Lac was divided into two segments taken at different times for operational reasons (Table 2). The 2 images of BL Lac were combined using the `CIAO` tool `mergeall` in order to increase the signal-to-noise ratio, for a total exposure of 3.1 ks.

4. Spatial analysis

The main aim of the spatial analysis is to investigate whether diffuse emission is present around the BL Lac objects or whether their X-ray radial profile is entirely consistent with a point source. In the latter case, no contribution to the local X-ray emission from a diffuse component is present.

The first step of the spatial analysis was to produce a smooth image of the field of view. For example, Fig. 1 shows the adaptively smoothed Chandra images of 1ES 2344+514 and PKS 0548-322, in the 0.3–8 keV energy range.

Before extracting the radial profiles of the sources, we removed from the images instrumental features (i.e., spikes produced by out-of-time events) and field sources. To find the field sources we used the detect tool `wavdetect` with the default value (10^{-9}) for the threshold for identifying a pixel as belonging to a source (see Sect. 7). For 3C 371, we also removed the X-ray jet (Pesce et al. 2001) by using an elliptical region ($1.6'' \times 1.1''$) centered on the jet. The same region was substituted by a region of identical shape and size located symmetrically with respect to the core, in order to restore a possible halo contribution.

Using the tools `dmextract` and `dmtcalc`, we extracted the radial profiles on a scale typical of clusters (i.e., approximately 250 kpc, see for example De Grandi et al. 1999) that correspond to a radius of about 200″ on our images, depending on the redshifts. In the case of the ACIS-I observations, this radius encompasses the boundary between the various CCDs. The estimated average influence of the gap between the single CCDs on the surface brightness is of the order of 4%, therefore the surface brightness should be considered as a lower limit. A series of annular regions, with increments of the radius of 2″, was used to extract the radial profile. For 3C 371, the only source observed with ACIS-S, the number of the annuli was limited by the distance between the source and the edge of S3.

While the responses of ACIS-I CCDs are not dramatically different, the response of S3 and S2 are different. The background regions were extracted from annular, circular, or box regions external to the annular regions centered on the sources. These regions are free of obvious sources.

In order to evaluate the instrumental response to a point source, we used the tool `mkpsf` to create an image of the Point Spread Function (PSF) of an on-axis point source, normalized to the source flux. The PSF changes with source position and photon energy, and is created by interpolation of the medium resolution library of pre-launch calibration files (the PSF hypercube library). The `mkpsf` tool is able to create only monochromatic PSFs. However, a monochromatic PSF is too simple a model to describe adequately the spatial distribution of our sources. We therefore improved the model to find a better representation of the source PSF, following a method similar to that used by Worrall et al. (2001). Our improvement consists on merging 8 different monochromatic PSFs chosen and weighted on the basis of the source energy spectra between 0.3 and 8 keV.

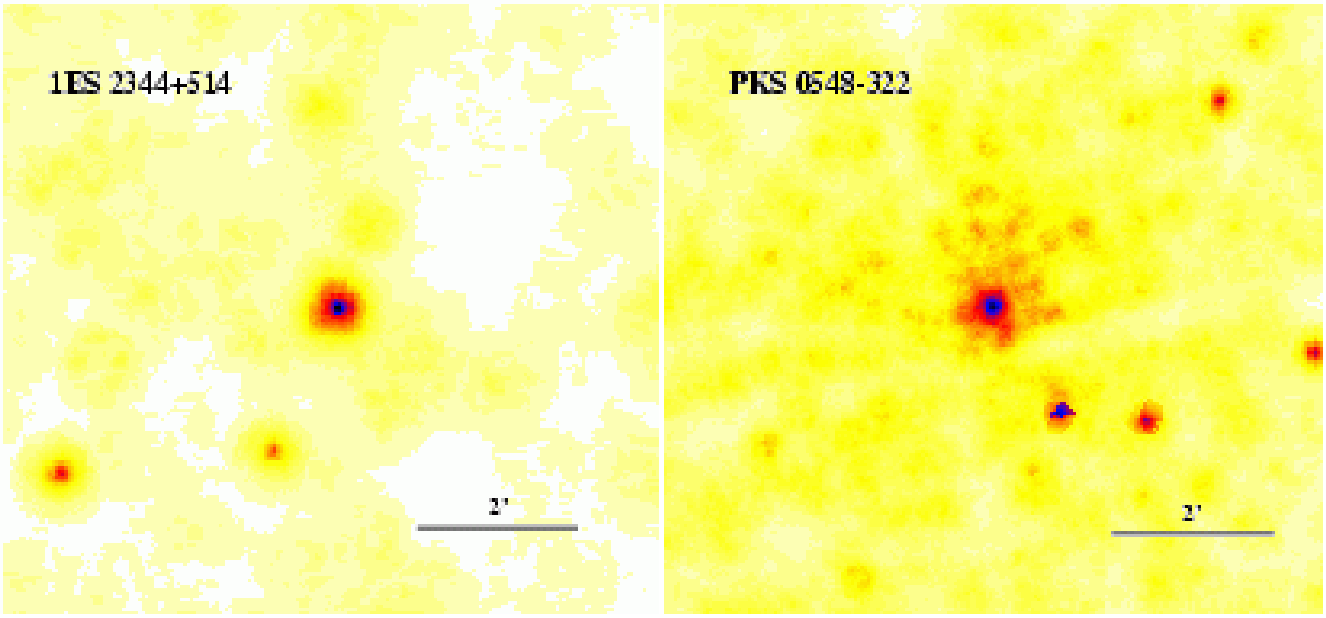

Fig. 1. Adaptively-smoothed *Chandra* ACIS-I images of 2 BL Lacs. North is up and East to the left. In PKS 0548–322, diffuse X-ray emission on cluster scales is apparent, while the image of 1ES 2344+514 exhibits a point source embedded in diffuse emission on the scale of the galaxy's halo.

This method can be summarized as follows:

1) We first extracted the energy distributions of the photons from a circular region centered on the source. The radii of these regions vary from 5″ to 10″, depending on the source brightness.

2) In each case, we sampled the entire photon distribution by choosing 8 discrete energy values. The number of counts at any of these energy values corresponds to the energy weight (see Fig. 2). The energies and weights are shown in Table 3 and are indicated with E and W, respectively.

3) Using `mkpsf` we created 8 monochromatic PSFs at the position of the AGN on the detector for each of the 8 sampled energies, and coadded them. Each PSF was weighted by its relative normalization (the weights).

Once we obtained the composite PSF, we searched for a fair analytical representation that describes it. This empirical representation is obtained using an 8-parameter function:

$$\mathrm{PSF}(x) = A_0 \left[A_1 \frac{\mathrm{e}^{-\frac{x}{A_2}}}{x^2} - A_3 + A_4 \mathrm{e}^{-\frac{(x-15)^2}{A_5}} + A_6 \mathrm{e}^{-\frac{(x-13)^2}{A_7}} \right]. \qquad (1)$$

For each source, we fitted the composite PSF with Eq. (1) and found the best-fit values of the 8 parameters (Table 4). The instrumental radial profile is not expected to be a good representation for the central region of strongly piled-up sources. Therefore, since no `CIAO` task exists yet to correct the PSF for pile-up, we normalized the instrumental radial profile at $r = 2''$: at larger distances the pile-up effect on the PSF is negligible, according to the *Chandra* Proposers' Observatory Guide. For each source we superimposed the composite PSF (weighted sum of the 8 monochromatic PSFs) on the surface brightness versus the radial distance.

Due to the pile-up effect on the spectral distribution of the photons (spectral hardening), this method is likely to overestimate the contribution of the hard photons. The result is a slightly broader PSF, which will not cause any false detection of extended emission but rather underestimate its contribution.

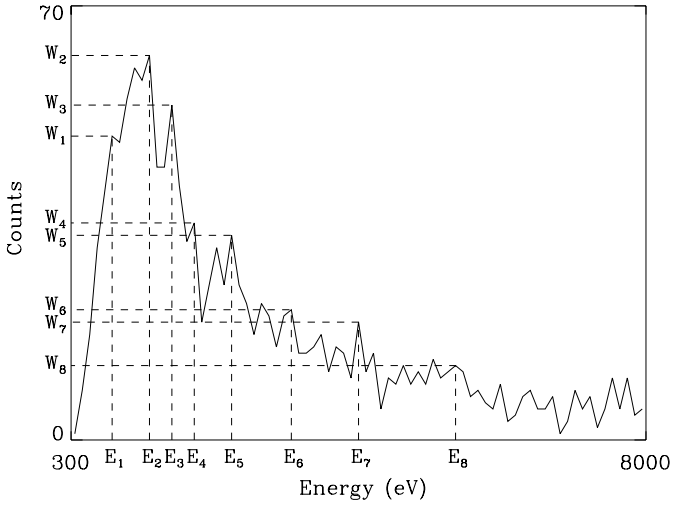

Fig. 2. Example of energy histogram for 1ES 2321+419, illustrating the procedure needed for the composite PSF (see text). The energies, *E*, and weights, *W*, for the monochromatic PSFs are indicated by the dashed lines.

After submitting this paper, a script that automatically performs the same task (`ChaRT`) was released by the *Chandra* X-ray Center (`CXC`). We performed the analysis of the radial profiles using `ChaRT` and found consistent results with our method above. In Fig. 3 we plot the radial profiles of the 6 sources. The dashed line indicates the profile of the composite PSF obtained using Eq. (1) and the parameters in Table 4. The horizontal dotted line represents the background.

In the case of 3C 371, the radial profile is consistent with the PSF and no excess emission is detected in our exposure.

Table 3. Energy weighting for the monochromatic PSFs.

Object Name (1)	E_1, W_1 (2)	E_2, W_2 (3)	E_3, W_3 (4)	E_4, W_4 (5)	E_5, W_5 (6)	E_6, W_6 (7)	E_7, W_7 (8)	E_8, W_8 (9)
PKS 0548–322	0.82, 34	1.22, 38	1.37, 30	1.62, 21	1.87, 19	2.07, 11	2.77, 8	3.47, 7
3C 371	0.47, 58	0.87, 58	1.17, 37	1.47, 37	1.87, 26	2.17, 23	2.72, 17	4.02, 10
PKS 2005–489	0.57, 77	0.87, 117	1.17, 102	1.27, 91	1.42, 70	1.52, 63	1.77, 38	1.97, 36
BL Lac	0.87, 7	1.22, 14	1.37, 10	1.62, 15	2.47, 8	3.07, 9	3.62, 6	4.17, 8
1ES 2321+419	0.77, 21	1.12, 28	1.32, 32	1.62, 28	1.92, 17	2.47, 16	2.92, 13	3.67, 11
1ES 2344+514	0.52, 5	1.02, 15	1.27, 15	1.52, 12	1.72, 7	2.17, 6	2.57, 6	4.82, 7

Columns: (1) = Source name; (2)−(9) = Energy (in keV) and weight of each monochromatic PSF that has been coadded in order to have a more realistic representation of the source PSF (see Sect. 4).

Table 4. PSF parameter values.

Object Name (1)	A_0 (2)	A_1 $\times 10^{-2}$ (3)	A_2 (4)	A_3 $\times 10^{-5}$ (5)	A_4 $\times 10^{-5}$ (6)	A_5 (7)	A_6 $\times 10^{-4}$ (8)	A_7 (9)
PKS 0548–322	0.17	5.5	5.2	0.5	0.7	0.34	1.4	12.5
3C 371	0.17	3.0	9.0	1.0	1.1	0.36	1.0	16.6
PKS 2005–489	0.29	6.5	10.0	3.7	4.8	0.09	2.0	12.0
BL Lac	0.30	2.0	7.1	14.0	0.2	0.02	1.8	70.0
1ES 2321+419	0.12	2.8	6.5	14.0	0.5	0.30	1.7	85.0
1ES 2344+514	0.32	3.0	9.0	4.5	1.0	1.64	0.8	15.0

Columns: (1) = Source name; (2)−(9) = Values of the parameters of the analytical function used to fit the composed PSF (see Sect. 4 and Eq. (1)).

In the case of BL Lac, 1ES 2321+419, and 1ES 2344+514, there is some evidence for weak excess emission between 18″ and 30″. Excess emission over the PSF is clearly present for PKS 0548–322 and PKS 2005–489 up to ∼150″ (180 kpc) and 130″ (160 kpc), respectively (Fig. 3).

A β-model (King profile) was used to model the excess X-ray emission in all cases. We find that the β model provides a significant improvement only in the case of BL Lac, PKS 0548–322, and PKS 2005–489. The free parameters of the β-model are the value of β and the core radius, r_c. For PKS 0548–322, the reduced χ^2 of the fit is $\chi^2_r = 1.23$ with 142 degrees of freedom (d.o.f.), with $\beta = 0.35 \pm 0.20$ and $r_c = 23.2'' \pm 2.5''$. For PKS 2005–489, $\chi^2_r = 1.0$ (138 d.o.f.), with $\beta = 0.56 \pm 0.08$ and $r_c = 12.1'' \pm 1.2''$. For BL Lac, the model parameters are poorly constrained; we thus fixed β to 0.6 (Worrall & Birkinshaw 1994) and left r_c as the only free parameter of the fit. We obtain $\chi^2_r = 0.94$ for 24 d.o.f. and $r_c = 14.7'' \pm 12.6''$. All the errors are 1σ.

The core radius implies a physical radius of the diffuse emission of 28 kpc in PKS 0548–322, 15 kpc in PKS 2005–489, and 18 kpc for BL Lac. These values are typical of the X-ray halo of the host galaxy (Birkinshaw et al. 2002; Fabbiano et al. 1992), which is a giant elliptical in all cases (Falomo & Kotilainen 1999). Figure 4 shows the PSF plus β model fit for PKS 0548–322 and PKS 2005–489, where the parameters are best constrained.

As is apparent from the observed radial profiles of PKS 0548–322 and PKS 2005–489, diffuse emission in these two sources extends well beyond the fitted value of the core radii, up to ∼130–150″, or several hundreds of kiloparsecs. This scale is typical of clusters, and indeed both sources are known to reside in optical clusters (Pesce et al. 1995). However, the radial profiles are suggestive of two components, one (the galaxy halo) up to 40″, plus a large-scale tail related to the cluster. Thus, we attempted a fit to the radial profiles with the PSF plus two β models. In the first model, the core radius was fixed to the halo radius of 23″ and 12″ for PKS 0548–322 and PKS 2005–489, respectively. The parameters of the second β-model were left free to vary. No improvement was obtained, and the core radius of the second β model is totally unconstrained. This is because the core radius of the cluster extends on a scale larger than our field of view, making its determination difficult. Thus, while the radial profiles show clear evidence for the presence of X-ray emission on cluster scales, it is not possible to constrain its spatial properties with the present data. However, given its isotropic distribution, the cluster X-ray emission dominates the X-ray spectrum, even when the latter is extracted on the scale of the galaxy halo (see below). Indeed, the cluster contribution is still present along the line of sight when extracting the spectrum on small spatial scales.

To evaluate the luminosities of the diffuse emission, we extracted the count rate from annular regions around the sources. For BL Lac, the annular region has inner and outer radii of 20″ and 35″, respectively. The measured 0.3–8 keV count rate is 0.011 ± 0.002 c/s. The count rate was converted into flux assuming a thermal Raymond-Smith spectrum with Galactic

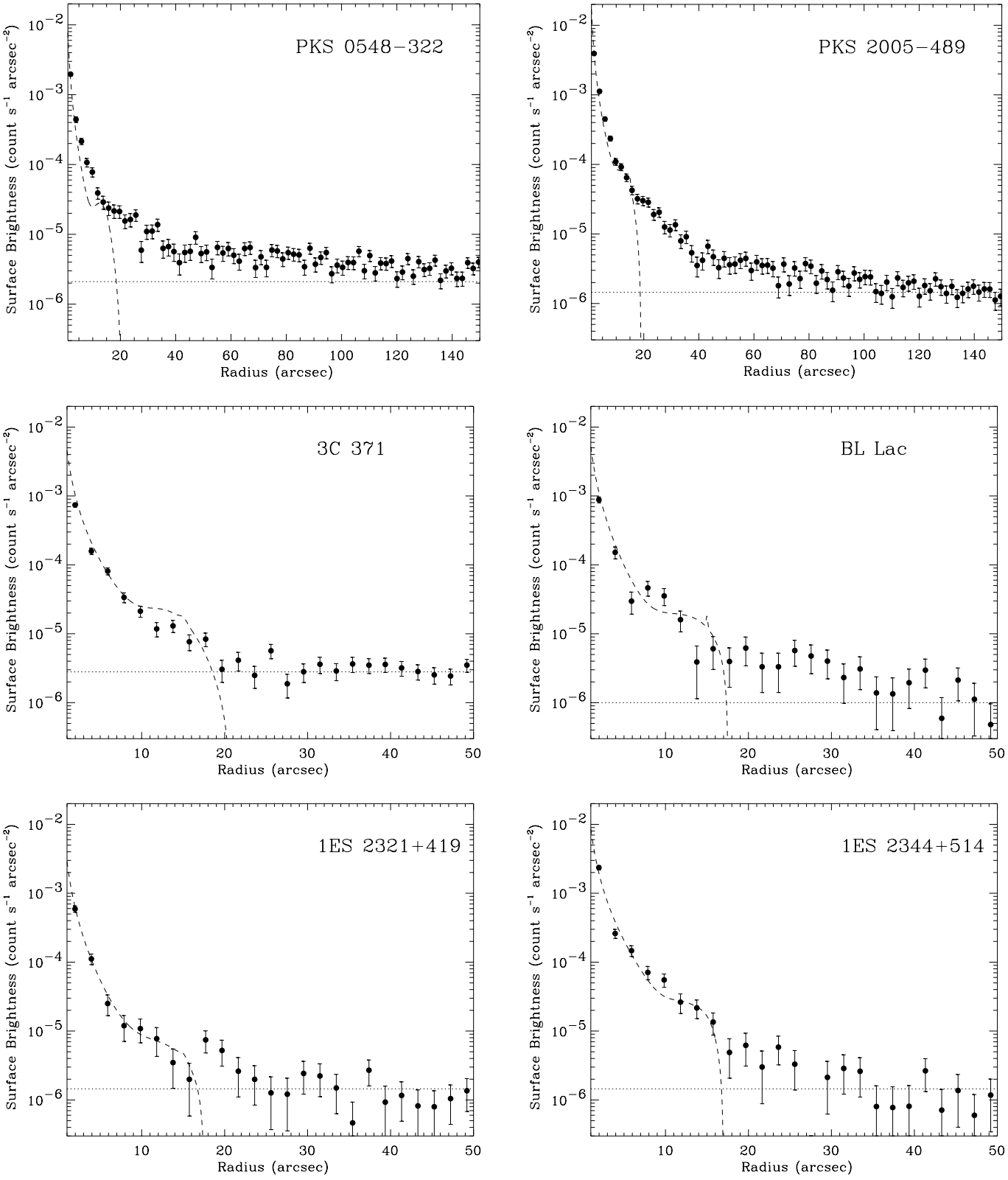

Fig. 3. ACIS radial profiles for each source of the sample (data points). The composite PSF, derived by merging several monochromatic PSFs (see text), is shown superimposed to the data (dashed line); the horizontal dotted line marks the background. For PKS 0548–322, PKS 2005–489, and BL Lac, excess X-ray counts over the PSF are present at radii $\gtrsim$20″, indicating diffuse X-ray emission around the core. Weak extended emission is also present for 1ES 2321+419 and 1ES 2344+514, while the profile for 3C 371 is entirely consistent with the instrumental PSF.

column density, temperature $kT = 1$ keV, and fixing abundances to 0.2 solar. The derived observed flux is $F_{0.4-5\ \mathrm{keV}} = 6.7 \times 10^{-14}$ erg cm^{-2} s^{-1}, corresponding to an absorption-corrected luminosity $L_{0.4-5\ \mathrm{keV}} = 1 \times 10^{42}$ erg s^{-1}, typical of FRIs halos (e.g., Worrall 2002).

For PKS 0548–322 and PKS 2005–489, the integrated count rate in 20″−40″ includes the contribution of the cluster. To evaluate the halo luminosity, we subtracted the cluster contribution from the total count rate in 20″−40″, rescaling the cluster surface brightness to the halo area and assuming a uniform cluster emission profile. We derive 0.019 ± 0.002 c/s and 0.038 ± 0.003 c/s in 0.3–8 keV for PKS 0548–322 and PKS 2005–489, respectively. Assuming a thermal Raymond-Smith spectrum with Galactic column density, temperature $kT = 1$ keV, and abundances fixed to 0.2 solar, these count rates correspond to an observed flux of $F_{0.4-5\ \mathrm{keV}} = 1.4 \times 10^{-13}$ erg cm^{-2} s^{-1} and intrinsic luminosity $L_{0.4-5\ \mathrm{keV}} = 1.3 \times 10^{42}$ erg s^{-1} for PKS 0548–322, and $F_{0.4-5\ \mathrm{keV}} = 3.1 \times 10^{-13}$ erg cm^{-2} s^{-1} and $L_{0.4-5\ \mathrm{keV}} = 3.1 \times 10^{42}$ erg s^{-1} for PKS 2005–489.

An alternative way to estimate the luminosity of the halo is based on the integration of the β-model over the extended component region. Integrating between 20″ and 40″ we obtained results fully consistent with those derived above. With this method, we can also evaluate the integrated luminosity over the entire 0″−40″ range. We found that the 0.4–5 keV unabsorbed fluxes for BL Lac, PKS 0548–322, and PKS 2005–489 are $F_{0.4-5\ \mathrm{keV}} = 2.8 \times 10^{-13}$ erg cm^{-2} s^{-1}, $F_{0.4-5\ \mathrm{keV}} = 3.3 \times 10^{-13}$ erg cm^{-2} s^{-1}, $F_{0.4-5\ \mathrm{keV}} = 7.6 \times 10^{-13}$ erg cm^{-2} s^{-1}, respectively. The corresponding intrinsic luminosities are $L_{0.4-5\ \mathrm{keV}} = 2.9 \times 10^{42}$ erg s^{-1} for BL Lac $L_{0.4-5\ \mathrm{keV}} = 3.3 \times 10^{42}$ erg s^{-1} for PKS 0548–322 $L_{0.4-5\ \mathrm{keV}} = 7.8 \times 10^{42}$ erg s^{-1} for PKS 2005–489.

The assumption of uniform cluster emission is unrealistic, as the cluster radial profile may increase toward the center of the cluster, where the gas is denser/hotter. Thus, the above count rates represent an upper limit to the X-ray emission of the galaxy's halo. For the cluster emission, the count rates extracted from 40″−150/130″ are 0.021 ± 0.002 c/s for PKS 0548–322, and 0.013 ± 0.001 c/s for PKS 2005–489. Assuming the parameters from the spectral analysis (see below), the corresponding observed fluxes and intrinsic luminosities are $F_{0.4-5\ \mathrm{keV}} = 2.9 \times 10^{-13}$ erg cm^{-2} s^{-1} and $L_{0.4-5\ \mathrm{keV}} = 3. \times 10^{42}$ erg s^{-1} for PKS 0548–322, and $F_{0.4-5\ \mathrm{keV}} = 1.3 \times 10^{-13}$ erg cm^{-2} s^{-1} and $L_{0.4-5\ \mathrm{keV}} = 1.3 \times 10^{42}$ erg s^{-1} for PKS 2005–489, typical of cluster with Abell richness 1 (Mulchaey & Zabludoff 1998; Mushotzky 1998; Mahdavi et al. 1997).

For 3C 371, 1ES 2321+419, and 1ES 2344+514, we evaluated upper limits to the extended halo. Count rates were extracted in an annulus of inner and outer radii 20″ and 40″, respectively, and converted into flux assuming a Raymond-Smith thermal model with $kT = 1$ keV, abundances fixed to 0.2 solar, and Galactic column densities. We derive $L_{0.4-5\ \mathrm{keV}} = 1.2 \times 10^{41}$ erg s^{-1} for 3C 371, $L_{0.4-5\ \mathrm{keV}} = 5.2 \times 10^{40}$ erg s^{-1} for 1ES 2321+419, and $L_{0.4-5\ \mathrm{keV}} = 4 \times 10^{40}$ erg s^{-1} for 1ES 2344+514.

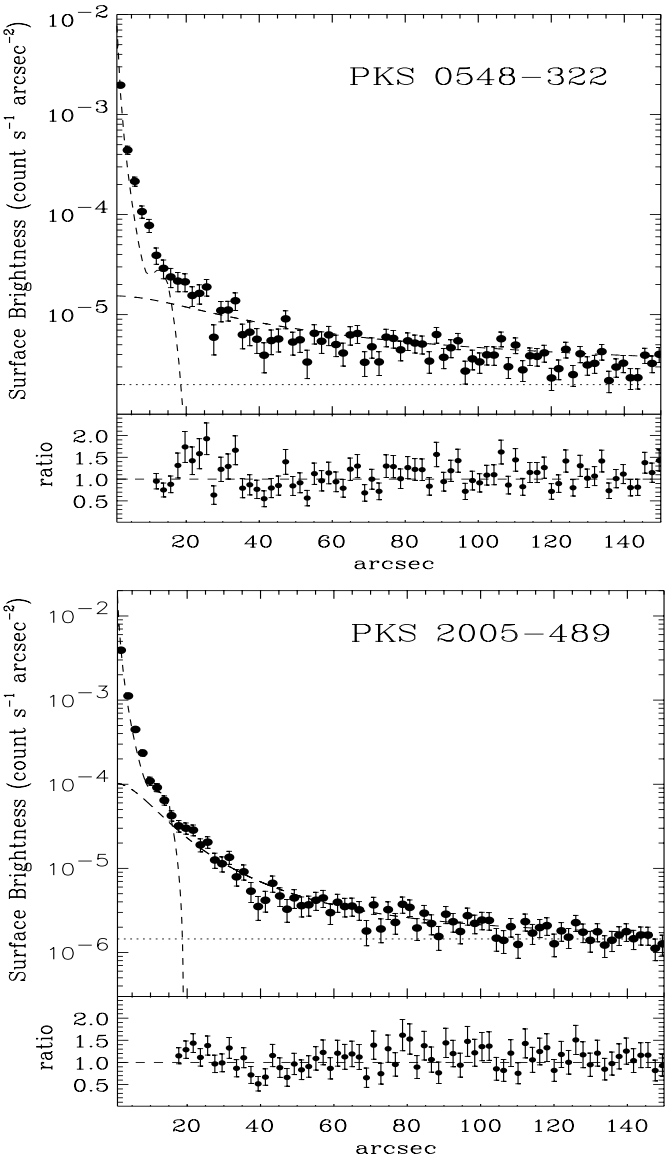

Fig. 4. Radial profiles and best-fit β-model for PKS 0548–322 and PKS 2005–489. In both cases, a single β-model was fitted to the data. However, two components for the diffuse emission are present, the first one on the scale of the host galaxy (~40″), and the second on the scale of the cluster (~130–150″). See text for further details.

In conclusion, diffuse X-ray emission is clearly present in 3 out of 6 sources of the sample (PKS 0548–322, PKS 2005–489, and BL Lac). In two other sources, 1ES 2321+419 and 1ES 2344+514, there is some weak evidence for faint diffuse emission. The diffuse emission in BL Lac, and possibly in the two 1ES sources, is on the scale of the galaxy's halo and has a luminosity typical of FRIs. In the two PKS sources, there is evidence for diffuse emission on both the galaxy halo and the cluster scale. However, it is not possible to model the cluster spatial properties.

5. Spectral analysis

The goal of this section is to investigate the X-ray properties of the diffuse X-ray emission in PKS 0548–322 and

PKS 2005–489. To this end, we extracted and analyzed the X-ray spectra of this component.

The ACIS-I spectra of the diffuse emission was extracted using an annulus centered on the core. We used a large extraction region (inner radius 20″, outer radius 150/130″) to increase the signal-to-noise ratio. We chose this high value for the inner radius in order to reduce contamination of the PSF wings from the AGN. An issue with such a large extraction region, however, is that it encompasses 4 CCDs that have different spectral responses. To circumvent this difficulty, we divided the extraction region in four sectors, each one covering a single CCD. The resulting four spectra were fitted jointly within XSPEC v.11.0.1. To account for the recently observed quantum efficiency decay of ACIS, possibly caused by molecular contamination of the ACIS filters, we have applied a time-dependent correction to the ACIS quantum efficiency based on the presently available information from the CXC[1].

The model used to fit the spectra is the thermal plasma model APEC, with column density fixed to the Galactic value (Table 1), solar abundances fixed at 0.2, and temperature kT ranging between 0 and 15 keV. We found $kT = 6.3^{+8.7}_{-2.8}$ keV, $\chi^2_{\rm r} = 0.42/47$, for PKS 0548–322, and $kT = 4.6^{+2.0}_{-1.7}$ keV, $\chi^2_{\rm red} = 0.97/54$ for PKS 2005–489. No improvements are obtained adding a second component (a power law or a second thermal model). The fitted temperatures are typical of the X-ray emission from the hot intracluster gas in rich cluster (De Grandi & Molendi 2002).

In an attempt to separate the contributions of the galaxy halo and of the cluster, we extracted two X-ray spectra, the first in the range 20″−40″ (to maximize the halo) and the second in 40″−130/150″, for both sources. We found that the best-fit is obtained using the APEC model and abundances fixed to 0.2 solar. Spectral analysis of the first spectrum shows that the fitted temperature (with range between 0 and 15 keV) is still high ($kT = 9.5^{+5.5}_{-4.6}$ keV with $\chi^2_{\rm r} = 0.62/6$ for PKS 0548–322 and $kT = 3.7^{+1.8}_{-1.3}$ keV with $\chi^2_{\rm r} = 0.90/18$ for PKS 2005–489), indicating that the cluster emission is still dominant. For the second spectrum, the parameters are: $kT = 6.0^{+9.0}_{-2.9}$ keV, $\chi^2_{\rm r} = 0.39/40$, for PKS 0548–322, and $kT = 12.1^{+2.9}_{-8.1}$ keV, $\chi^2_{\rm r} = 0.98/34$ for PKS 2005–489.

6. Summary and conclusions

We presented *Chandra* ACIS-I/S observations of 6 BL Lacertae objects (four HBLs and two LBLs), aimed at detecting the diffuse circumnuclear X-ray emission predicted by the unification models. The short exposures, 2–6 ks (10 ks for 3C 371), were optimized to detect diffuse emission, but are insufficient to study their properties in detail.

Diffuse X-ray emission was convincingly detected in 3/6 cases (PKS 0548–322, PKS 2005–489, and BL Lac), with marginal evidence in an additional 2 sources (1ES 2321+419 and 1ES 2344+514). The extended X-ray emission is on scales of several kiloparsec and has a luminosity similar to FRI galaxies studied with *Chandra* (Worrall et al. 2002). This qualitatively supports the unification models for radio-loud AGN, which states that BL Lacs and FRI galaxies are the same intrinsic objects, seen at different orientations of the relativistic jets, with BL Lacs being the sources more closely aligned with the line of sight.

The presence of an extended X-ray emission around the X-ray cores, interpreted as a thermal bremsstrahlung from a galactic atmosphere, can trace the medium whose pressure may confine the jets that are pointing toward us. For PKS 0548–322 and PKS 2005–489 we evaluated the density and the external pressure of the X-ray component. The gas density profile is derived by deprojection of the β-model used for the decomposition of the surface brightness profile (e.g., Ettori 2000). We adopted the cooling function value (e.g., Sarazin 1988) for the hot gas temperature and abundance derived from the spectral analysis. The resulting central gas density is 1.4×10^{-3} atoms cm^{-3} for PKS 0548–322 and 7.4×10^{-3} atoms cm^{-3} for PKS 2005–489. The external pressures evaluated at the characteristic radii (28 kpc for PKS 0548–322 and 15 kpc for PKS 2005–489) are $P_{\rm ext} = 5.2 \times 10^{-14}$ N m^{-2} and $P_{\rm ext} = 2.2 \times 10^{-13}$ N m^{-2}, respectively.

Comparing the external gas pressure to the internal jet pressure can provide useful information on the propagation of the jet. As the jets of BL Lacertae objects are seen at small angles with respect to the line of sight, the internal jet pressure can only be derived via modeling of the SED of the blazar. Ghisellini et al. (2002) estimated the total jet pressure for a sample of blazars, including FSRQs, LBLs, and HBLs. In the case of our sources (considered extreme HBLs), the inferred pressure ranges from $\sim 2 \times 10^{-3}$ N m^{-2} to $\sim 6 \times 10^{-2}$ N m^{-2} (Fig. 2 of Ghisellini et al. 2002). These are several orders of magnitude larger than the external gas pressure, implying the jets cannot be confined by the external pressure of the galactic atmosphere, at least on parsec scales. This is not unexpected, since it is commonly accepted that the jets start out supersonic near the central black hole.

One of the goals of the *Chandra* observations was to determine whether HBLs and LBLs are characterized by different environments. The two classes exhibit different properties in terms of their Spectral Energy Distributions (e.g., Donato et al. 2001 and references therein), and the decreasing luminosity from LBLs to HBLs can be interpreted as a reduction in the jet power from the central energy source. One can thus ask the question of whether the difference in jet power in HBLs and LBLs is due to different gaseous environments. For example, one could hypothesize that the less powerful HBL jets live in a denser medium that is more efficient in decelerating them. Unfortunately, the present sample is insufficient to draw firm conclusions: of the 5 sources exhibiting diffuse X-ray emission, 4 are HBLs and only 1 is an LBL. More fundamentally, the short ACIS exposure prevents us from a detailed spectral analysis of the circumnuclear gas. Deeper follow-up *Chandra* observations are needed to this aim, as well as a larger, statistical sample of both HBLs and LBLs. On the optical side, we note that recent *HST* observations reveal no differences in the host galaxy properties of the two BL Lac subclasses (Urry et al. 2000; Scarpa et al. 2000).

[1] `http://cxc.harvard.edu/ciao/threads/apply_acisabs/index.html`

Diffuse X-ray emission on scales of 100 kpc or more, typical of a cluster of galaxies, is present in PKS 0548–322 and PKS 2005–489. This finding independently confirms previous claims, based on optical imaging, that these two BL Lacs reside in clusters of moderate-to-poor richness. However, the spatial parameters of the X-ray emission of the cluster are unconstrained in our ACIS images, while the X-ray emission of the cluster gas dominates the spectrum integrated along the line of sight. The cluster temperature and luminosity appears consistent (within 2σ) with the values found for normal clusters, i.e., clusters with no AGN activity (e.g., Mahdavi et al. 1997; Mulchaey & Zabludoff 1998; Mushotzky 1998; Markevitch 1998), suggesting that the presence of the AGN does not affect the global properties of the gas. On the other hand, it is also interesting that the two brightest X-ray BL Lacs of the sample reside in an extended environment, suggesting that the gas can affect nuclear activity. For example, Ellingson et al. (1991) suggested that nuclear activity could be triggered by galaxy-galaxy interactions and merging in the cluster core. Such a possibility is supported in the case of PKS 0548–322 by the presence of tidal interactions between the host galaxy of the BL Lac and nearby companion galaxies as seen in the optical image (Falomo et al. 1995).

In conclusion, we detected diffuse X-ray emission around the cores of 3, and possibly 5, BL Lacertae objects within our short *Chandra* exposures. The core radii and luminosities of the diffuse X-ray emission are similar to those observed in FRI radio galaxies. This finding supports current unification models for radio-loud AGN, which attempt at unifying BL Lacs and FRI galaxies through orientation. Future work will include deeper and additional X-ray observations of a larger, statistical sample of BL Lacs, in order to put this conclusion on a firmer basis and to determine in greater detail the physical properties of the diffuse gas.

Acknowledgements. We thank the referee, Dr. M. J. Hardcastle, for the useful comments and suggestions that improved the paper. We gratefully acknowledge financial support from NASA grants NAG5-10073 (DD, RMS), NAS8-39073 (JEP), and LTSA grant NAG5-10708 (MG, RMS). This research made use of the NASA/IPAC Extragalactic Database (NED) which is operated by the Jet Propulsion Laboratory, Caltech, under contract with the National Aeronautics and Space Administration.

Appendix A: Serendipitous sources in the *Chandra* fields

A glance at the *Chandra* images reveals the presence of several point sources in the fields of the targets. We used the `CIAO` tool `wavdetect` to search for serendipitous X-ray sources in the f.o.v. In the algorithm, the parameter `scale` (a list of radii, in image pixels, of Mexican Hat wavelet functions) was left free to range between 1 and 16, and the parameter `threshold` (the number of detected spurious sources in a pixel map) held fixed at 10^{-9}. The algorithm returns a list of elliptical regions that define the positions and the shapes of the detected sources. We next used the coordinates from `wavdetect` and its associated error regions to search for their optical counterparts on ESO archival plates. We used circular search regions with radii of 5″ because it is known that most reprocessed ACIS-I observations have an offset of up to 1.5″[2].

In Table 5 we list the coordinates (J2000), the net counts, and the detection significance in σ, where σ is the ratio of the net source counts to the "Gehrels error" of the background counts (for more details, see `wavdetect` manual at the following URL `http://asc.harvard.edu/toolkit/pimms.jsp`). We report the hardness ratios, defined as the difference between the count rates in the 2–8 keV (hard band) and those in the 0.3–2 keV (soft band), divided by the 0.3–8 keV count rate. A positive value of the hardness ratio suggests that the source has a flat spectrum, while a positive value suggests a steep spectrum. Also listed in Table 5 are the ESO identification codes, the angular distance of the optical source from the X-ray source, and the apparent magnitudes in the red and blue bands. The NED and Simbad on-line catalogs were searched to find additional information on the optical counterparts.

We now comment on individual *Chandra* fields.

PKS 0548–322: In the *Chandra* field we found 7 serendipitous point sources (Table 5). Optical counterparts are found for all sources, except source G (see Fig. 5, left, for the overlay of the X-ray isocontours on the optical image). The X-ray sources detected with `wavdetect` are marked with capital letters. Source E coincides with 1WGA J0550.3-3216, an X-ray source previously identified by the *ROSAT* satellite. Source B is a galaxy from the 2MASS catalog (2MASXi J0550366-321733), studied in previous optical works (Pesce et al. 1995; Falomo et al. 1995). This spiral galaxy coincides with galaxy G4 in the PKS 0548–322 cluster (Falomo et al. 1995), and has a redshift of $z = 0.072$. Falomo et al. (1995) found strong emission lines in the optical spectrum and classified the source as an extreme Fe II emitting AGN. We measure ∼200 X-ray counts from the nucleus of this galaxy in the energy range 0.3–8 keV, sufficient for a crude spectral analysis. The X-ray spectrum is well fitted ($\chi^2_r = 1.37/16$) by a single power law with absorption fixed to Galactic, and photon index $\Gamma = 2.21 \pm 0.33$. This is consistent with the canonical slope of $\Gamma = 1.8$ measured for Seyferts and other lower-luminosity AGN. The observed 2–10 keV flux is $F_{2-10\ \mathrm{keV}} = 1.4 \times 10^{-13}$ ergs cm^{-2} s^{-1}, corresponding to an intrinsic luminosity of $L_{2-10\ \mathrm{keV}} = 1.4 \times 10^{42}$ erg s^{-1}, assuming a redshift of 0.072.

3C 371: The Western elongation of the soft X-ray emission in Fig. 1 is due to the X-ray jet (Pesce et al. 2001). Seven X-ray sources are detected in the *Chandra* field but only two sources, B and G, have an optical counterpart.

PKS 2005–489: In the X-ray image we detected 7 point sources. Sources D, E, and F have very weak optical counterparts, and source C corresponds to a F8V double or multiple star (CCDM J20091-4856AB also called HD 190857). For the positions of the detected X-ray sources on the optical image, see Fig. 5, right.

BL Lac: Ten serendipitous sources are detected in the *Chandra* field. Only four of them (A, B, F, and H) have optical counterparts.

[2] See the memo on astrometry problems at `http://cxc.harvard.edu/mta/ASPECT/improve_astrometry.html`

Table 5. Field sources.

(1)	RA (2)	Dec (3)	c/s (4)	HR (5)	(σ) (6)	ESO Code (7)	Dist. (8)	M_R (9)	M_B (10)	Note (11)
	PKS 0548–322									
A	05 50 52.17	–32 10 52.5	91	–0.65	36.85	U0525-02418996	0.560	16.3	16.8	
B	05 50 36.63	–32 17 33.3	193	–0.59	74.42	U0525-02415715	0.406	14.6	14.8	(a)
C	05 50 31.50	–32 17 39.2	28	–0.86	11.49	U0525-02414666	0.506	17.8	20.1	
D	05 50 27.25	–32 13 49.0	17	–0.65	7.62	U0525-02413729	0.563	18.1	20.7	
E	05 50 21.63	–32 16 49.4	18	–0.22	7.97	U0525-02412549	0.727	17.9	18.9	(b)
F	05 51 14.78	–32 13 03.4	12	–0.83	5.12	U0525-02423572	1.284	11.9	12.0	
G	05 51 13.26	–32 25 47.5	32	0.06	11.11	–	–	–	–	
	3C 371									
A	18 07 37.87	69 51 12.1	8	0.00	3.61	–	–	–	–	
B	18 07 26.57	69 46 26.6	38	–0.79	11.26	U1575-03911444	0.521	19.2	19.2	
C	18 07 04.30	69 49 32.8	7	0.14	2.88	–	–	–	–	
D	18 06 50.17	69 46 23.1	7	–1.00	2.59	–	–	–	–	
E	18 07 27.11	69 45 32.1	28	–0.79	7.87	–	–	–	–	
F	18 06 58.78	69 43 59.0	36	–0.17	10.59	–	–	–	–	
G	18 06 03.36	69 51 17.4	19	–0.79	7.34	U1575-03907608	1.382	16.9	19.3	
	PKS 2005–489									
A	20 09 41.06	–48 47 22.9	8	–0.25	3.76	–	–	–	–	
B	20 09 13.88	–48 46 38.0	8	–0.25	3.74	–	–	–	–	
C	20 09 07.14	–48 55 35.2	33	–1.00	14.55	U0375-38531345	0.385	9.7	11.4	(c)
D	20 09 52.53	–48 56 08.9	30	–0.20	12.43	U0375-38543383	0.536	18.2	19.0	
E	20 09 36.39	–48 42 02.9	11	–0.27	4.59	U0375-38539109	1.104	18.2	19.4	
F	20 09 30.34	–48 56 19.8	7	–0.71	3.53	U0375-38537485	1.560	18.2	19.9	
G	20 08 30.15	–48 50 33.2	17	–0.53	6.06	–	–	–	–	
	BL LAC									
A	22 02 53.68	42 17 48.5	32	–0.94	16.11	U1275-16943177	2.131	13.0	14.5	
B	22 02 51.03	42 13 02.2	15	–0.07	7.28	U1275-16942082	0.588	18.0	18.2	
C	22 02 43.81	42 13 45.3	9	0.56	4.90	–	–	–	–	
D	22 02 14.64	42 13 53.4	38	–0.58	18.69	–	–	–	–	
E	22 03 11.04	42 14 36.9	10	–0.20	4.83	–	–	–	–	
F	22 03 09.86	42 13 37.0	6	–0.33	3.40	U1275-16950337	0.420	13.9	15.0	
G	22 03 03.50	42 14 01.2	8	–0.50	4.22	–	–	–	–	
H	22 02 54.06	42 11 03.6	19	–0.26	8.94	U1275-16943366	2.604	17.4	18.1	
I	22 02 30.81	42 11 29.2	7	0.14	3.32	–	–	–	–	
L	22 02 18.88	42 22 28.9	41	0.07	1.88	–	–	–	–	
	1ES 2321+514									
A	23 24 06.48	42 11 52.9	16	0.12	8.27	–	–	–	–	
B	23 23 40.64	42 05 29.0	13	0.38	6.34	U1275-18369935	0.463	17.9	18.6	
C	23 23 35.36	42 05 51.8	18	–0.78	8.70	–	–	–	–	
D	23 23 33.08	42 07 42.1	9	–0.33	4.18	–	–	–	–	
E	23 24 16.16	42 14 28.7	12	–0.33	5.94	–	–	–	–	
F	23 24 02.15	42 05 21.2	8	0.50	4.25	U1275-18374011	1.440	16.4	17.1	
G	23 23 27.33	42 08 45.9	8	0.25	3.57	–	–	–	–	
H	23 24 01.26	42 00 46.5	18	–0.56	6.13	–	–	–	–	
I	23 23 43.62	42 01 44.4	13	–0.54	5.22	U1275-18370478	3.179	18.4	18.6	
L	23 23 26.60	42 05 53.7	13	–0.54	5.51	–	–	–	–	
M	23 23 11.51	42 06 36.6	17	–0.53	5.69	–	–	–	–	
	1ES 2344+514									
A	23 47 27.14	51 40 18.4	9	–0.56	5.56	U1350-18688025	1.522	18.7	19.1	
B	23 47 10.40	51 40 32.3	8	–0.25	3.90	U1350-18682932	0.944	16.5	17.9	
C	23 46 36.64	51 42 30.5	16	–0.50	7.86	–	–	–	–	
D	23 47 34.55	51 43 52.2	7	–1.00	3.36	U1350-18690283	0.840	11.2	11.8	(d)
E	23 47 23.94	51 41 36.8	7	–0.43	3.47	–	–	–	–	
F	23 48 06.02	51 40 16.9	9	–0.56	4.18	–	–	–	–	
G	23 47 32.77	51 34 42.0	4	–1.00	1.81	–	–	–	–	

Columns: (1) = Detected source; (2) = Right Ascension at J2000; (3) = Declination at J2000; (4) = Net count rate in 0.3–8 keV; (5) = Hardness Ratio, defined as $(h - s)/(h + s)$ where h is the count rate in 2–8 keV and s in 0.3–2 keV; (6) = Detection significance (in σ, see Sect. 7); (7) = ESO identification code; (8) = Distance (in $''$) between the Chandra coordinate and the optical one; (9)–(10) = Optical magnitude in the red and blue band; (11) = (a) Galaxy 2MASXi J0550366-321733; (b) ROSAT X-ray source 1WGA J0550.3-3216 XrayS; (c) Star CCDM J20091-4856AB or HD 190857; (d) Star GSC 03650-00158.

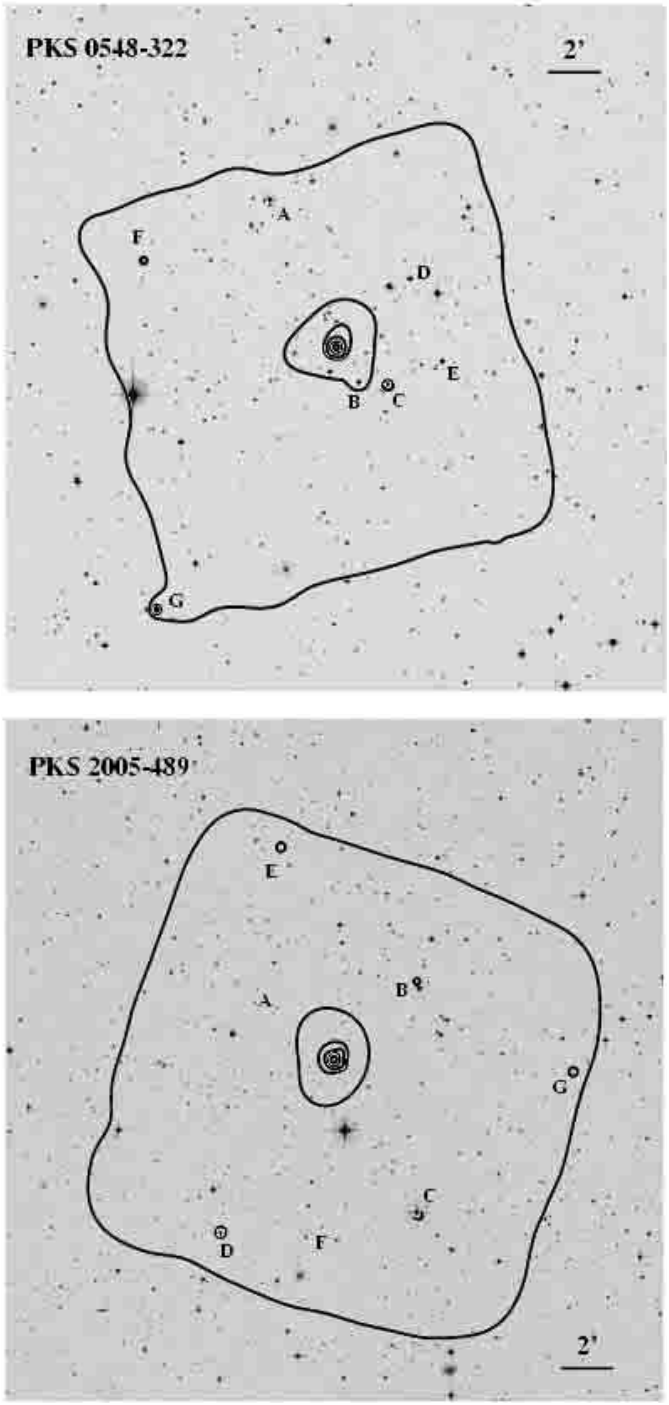

Fig. 5. X-ray contours in the energy range 0.3–8 keV overlaid on the optical images obtained from the 2.4 m Mount Palomar Telescope (POSS) archive for PKS 0548–322 (top) and PKS 2005–489 (bottom). The serendipitous X-ray sources detected with `wavdetect` (see text and Table 5) are marked with capital letters. North is to the top and East to the left.

1ES 2321+419: Eleven field sources are detected. Only three of them (B, F, and I) have optical counterparts.

1ES 2344+514: Seven X-ray sources are found in this *Chandra* field. The weak X-ray source D coincides with a bright star (GSC 03650-00158).

References

Antonucci, R. 1993, ARA&A, 31, 473
Barthel, P. D. 1989, ApJ, 336, 606
Birkinshaw, M., Worrall, D. M., & Hardcastle, M. J. 2002, MNRAS, 335, 142
Canosa, C. M., Worrall, D. M., Hardcastle, M. J., & Birkinshaw, M. 1999, MNRAS, 310, 30
De Grandi, S., Böhringer, H., Guzzo, L., et al. 1999, ApJ, 514, 148
De Grandi, S., & Molendi, S. 2002, ApJ, 567, 163
Dickey J. M., & Lockman, F. J. 1990, ARA&A, 28, 215
Donato, D., Ghisellini, G., Tagliaferri, G., & Fossati, G. 2001, A&A, 375, 739
Ellingson, E., Yee, H. K. C., & Green, R. F. 1991, ApJ, 371, 49
Ettori, S. 2000, MNRAS, 311, 313
Fabbiano, G., Kim, D.-W., & Trinchieri, G. 1992, ApJS, 80, 531
Falomo, R., & Kotilainen, J. K. 1999, A&A, 352, 85
Falomo, R., Pesce, J. E., & Treves, A. 1995, ApJ, 438, L9
Fossati, G., Maraschi, L., Celotti, A., Comastri, A., & Ghisellini, G. 1997, MNRAS, 289, 136
Ghisellini, G., Celotti, A., & Costamante, L. 2002, A&A, 386, 833
Giommi, P., Barr, P., Pollock, A. M. T., Garilli, B., & Maccagni, D. 1990, ApJ, 356, 432
Hardcastle, M. J., Worrall, D. M., & Birkinshaw, M. 1999, MNRAS, 305, 246
Kollgaard, R. I., Wardle, J. F. C., Roberts, D. H., & Gabuzda, D. C. 1992, AJ, 104, 1687
Kubo, H., Takahashi, T., Madejski, G., et al. 1998, ApJ, 504, 693
Mahdavi, A., Böehringer, H., Geller, M. J., & Ramella, M. 1997, ApJ, 483, 68
Markevitch, M. 1998, ApJ, 504, 27
Mulchaey, J. S., & Zabludoff, A. I. 1998, ApJ, 496, 73
Mushotzky, R. 1998, PNAS, 95, 72
Padovani, P., & Giommi, P. 1995, ApJ, 444, 567
Padovani, P., & Urry, C. M. 1991, ApJ, 368, 373
Padovani, P., Costamante, L., Giommi, P., et al. 2001, MNRAS, 328, 931
Perlman, E. S., Stocke, J. T., Schachter, J. F., et al. 1996, ApJS, 104, 251
Pesce, J. E., Falomo, R., & Treves, A. 1995, AJ, 110, 1554
Pesce, J. E., Sambruna, R. M., Urry, C. M., & Scarpa, R. 2000, HEAD, 32.0302
Pesce, J. E., Sambruna, R. M., Tavecchio, F., et al. 2001, ApJ, 556, L79
Ravasio, M., Tagliaferri, G., Ghisellini, G., et al. 2002, A&A, 383, 763
Sambruna, R. M., Maraschi, L., & Urry, C. M. 1996, ApJ, 463, 444
Sambruna, R. M., Maraschi, L., Tavecchio, F., et al. 2002, ApJ, 571, 206
Scarpa, R., Urry, C. M., Falomo, R., Pesce, J. E., & Treves, A. 2000, ApJ, 532, 740
Sarazin, C. L. 1988, X-ray emission from clusters of galaxies (Cambridge University Press)
Urry, C. M., & Padovani, P. 1995, PASP, 107, 803
Urry, C. M., Padovani, P., & Stickel, M. 1991, ApJ, 382, 501
Urry, C. M., Scarpa, R., O'Dowd, et al. 2000, ApJ, 532, 816
Veron-Cetty, M.-P., & Veron, P. 2001, A&A, 374, 92
Worrall, D. M. 2002, NewAR, 46, 121
Worrall, D. M., & Birkinshaw, M. 1994, ApJ, 427, 134
Worrall, D. M., & Birkinshaw, M. 2000, ApJ, 530, 178
Worrall, D. M., Birkinshaw, M., & Hardcastle, M. J. 2001, MNRAS, 326, L7
Wurtz, R., Stocke, J. T., Ellingson, E., & Yee, H. K. C. 1997, ApJ, 480, 547